View Online / Journal Homepage / Table of Contents for this issue
Dynamic Article Links

PCCP

Cite this: *Phys. Chem. Chem. Phys.*, 2012, **14**, 4204–4216

www.rsc.org/pccp

PAPER

Multi-structural variational transition state theory: kinetics of the 1,5-hydrogen shift isomerization of the 1-butoxyl radical including all structures and torsional anharmonicity†

Xuefei Xu, Ewa Papajak, Jingjing Zheng and Donald G. Truhlar*

Received 22nd November 2011, Accepted 16th January 2012
DOI: 10.1039/c2cp23692c

Published on 16 January 2012 on http://pubs.rsc.org | doi:10.1039/C2CP23692C
Downloaded by University of Minnesota - Twin Cities on 04 March 2012

We investigate the statistical thermodynamics and kinetics of the 1,5-hydrogen shift isomerization reaction of the 1-butoxyl radical and its reverse isomerization. The partition functions and thermodynamic functions (entropy, enthalpy, heat capacity, and Gibbs free energy) are calculated using the multi-structural torsional (MS-T) anharmonicity method including all structures for three species (reactant, product, and transition state) involved in the reaction. The calculated thermodynamic quantities have been compared to those estimated by the empirical group additivity (GA) method. The kinetics of the unimolecular isomerization reaction was investigated using multi-structural canonical variational transition state theory (MS-CVT) including both multiple-structure and torsional (MS-T) anharmonicity effects. In these calculations, multidimensional tunneling (MT) probabilities were evaluated by the small-curvature tunneling (SCT) approximation and compared to results obtained with the zero-curvature tunneling (ZCT) approximation. The high-pressure-limit rate constants for both the forward and reverse reactions are reported as calculated by MS-CVT/MT, where MT can be ZCT or SCT. Comparison with the rate constants obtained by the single-structural harmonic oscillator (SS-HO) approximation shows the importance of anharmonicity in the rate constants of these reactions, and the effect of multi-structural anharmonicity is found to be very large. Whereas the tunneling effect increases the rate constants, the MS-T anharmonicity decreases them at all temperatures. The two effects counteract each other at temperatures 385 K and 264 K for forward and reverse reactions, respectively, and tunneling dominates at lower temperatures while MS-T anharmonicity has a larger effect at higher temperatures. The multi-structural torsional anharmonicity effect reduces the final reverse reaction rate constants by a much larger factor than it does to the forward ones as a result of the existence of more low-energy structures of the product 4-hydroxy-1-butyl radical than the reactant 1-butoxyl radical. As a consequence there is also a very large effect on the equilibrium constant. The neglect of multi-structural anharmonicity will lead to large errors in the estimation of reverse reaction rate constants.

1. Introduction

Alkoxyl radicals as key intermediate species play important roles in both combustion and atmospheric chemistry.[1] Once formed, the relative rates and branching ratios of their subsequent reactions,[2] which could be decomposition, isomerization, and reactions with other molecules or radicals, will strongly affect the distribution of final products. Hence, both the knowledge of the thermodynamics of these radicals and accurate measurement or calculation of the kinetics of these radical reactions are very important for developing mechanisms of combustion and atmospheric processes. However, the corresponding experimental studies of the thermodynamics (or the properties required to for statistical thermodynamics) and reaction kinetics of reactive radicals are very hard, especially in the gas phase.

In the present work, we present a theoretical and computational study of the 1,5-hydrogen shift isomerization reaction of the 1-butoxyl radical. The 1-butoxyl radical is an important radical in the combustion of the biofuel 1-butanol. As the dominant reaction channel of the 1-butoxyl radical, the 1,5-hydrogen shift isomerization rate has been investigated by both experimental[3] and theoretical[4] methods. Due to the short lifetime and difficulty of detection of radicals, the experimental isomerization rate is usually obtained indirectly and over a limited temperature range. For example, Cassanelli *et al.*[3d] measured the branching ratio between the 1,5-hydrogen shift isomerization reaction of 1-butoxyl

Department of Chemistry and Supercomputing Institute, University of Minnesota, Minneapolis, MN 55455-0431, USA. E-mail: truhlar@umn.edu

† Electronic supplementary information (ESI) available: Structures of the reactant, product, and transition state and modified MM3 parameters. See DOI: 10.1039/c2cp23692c

 This journal is © the Owner Societies 2012

Published on 16 January 2012 on http://pubs.rsc.org | doi:10.1039/C2CP23692C
Downloaded by University of Minnesota - Twin Cities on 04 March 2012

and the reaction of 1-butoxyl with O_2 as a function of oxygen concentration at atmospheric pressure over the temperature range 250–318 K, then converted the rate constant ratio to an absolute rate constant for isomerization reaction by using the temperature-dependent absolute rate constant of the O_2 reaction. Heiss and Sahetchian[3b] derived the isomerization rate of the 1-butoxyl radical over 343–503 K from the ratio of the isomerization rate to the decomposition rate of 1-butoxyl and the known decomposition rate. Theoretical modeling extends the rate constant estimation to a larger temperature range, and—if accurate enough—can provide either a check on the experimental results or an improvement on them. In previous theoretical studies, Somnitz[4e] obtained consistent results with Cassanelli *et al.*'s experimental rate constants at low temperatures by using RRKM theory including tunneling contributions calculated with the assumption of conservation of vibrational energy and with a fully coupled multiple-channel master equation (ME). A study[4f] by two of us employed single-structure variational transition state theory (SS-VTST)[5] with the small-curvature tunneling[6] (SCT) approximation and concluded that Somnitz had underestimated the tunneling. However the SS-VTST calculated rate constants[4f] have large deviations from Cassanelli *et al.*'s results at low temperature, and the same divergence is noticed in the study of Davis and Francisco[4g] with a small-curvature parabolic approximation for tunneling[7] and G4[8] electronic structure calculations. These discrepancies could result in part from both the two studies not accounting for the anharmonicity in calculations of partition functions. In addition, in a later section we will mention that Davis and Francisco[4g] also significantly overestimated tunneling with the parabolic tunneling approximation and underestimated tunneling with the Wigner method[9] at low temperature.

Both the reactant 1-butoxyl radical and the product 4-hydroxy-1-butyl have more than one torsion. The presence of multiple torsional degrees of freedom often results in multiple minima on the potential energy surface, which results in multiple-structure anharmonicity. The reactant 1-butoxyl radical has three torsional motions. One of them is the torsion of a methyl group, which does not generate additional distinguishable structures, and each of other two torsional motions can generate three (one *trans* (T) and two *gauche* (G)) structures, so that ideally $3 \times 3 = 9$ distinguishable structures would be generated for 1-butoxyl. In previous theoretical studies that only considered a single structure, Somnitz[4e] and Méreau *et al.*[4b] used a GT structure for 1-butoxyl (in Fig. 1, this is the structure in which the O–C–C–C torsion is *gauche*, and the C–C–C–C torsion is *trans*); two of us[4f] and Davis and Francisco[4g] used only the TT structure (fourth structure in Fig. 1). In the present study, as discussed more fully below, we located ten conformers (five pairs of mirror images) with the M08-SO density functional. The ten conformers are close to each other in energy, and the largest energy difference, before including zero point energy, is only 0.69 kcal mol^{-1}. Because the structures are all low in energy, they can all play an important role in calculations of partition functions. We found that the ratio between the partition functions calculated with the multi-structural torsional approximation[10] (MS-T), including both multiple-structure anharmonicity and torsional anharmonicity, and those calculated in the single-structure harmonic-oscillator (SS-HO) approximation is as much as a factor of 11.5 for 1-butoxyl. The inaccuracy in partition functions calculations that do not include multiple-structure anharmonicity leads to large errors in the theoretical prediction of thermochemical properties (such as equilibrium constants) and rate constants.

The work in 2003 by Vereecken and Peeters[4c] has been so far the only theoretical study incorporating multiple conformers of the reactant and the transition state for the 1,5-H-shift isomerization reaction of 1-butoxyl. They reported that the temperature dependence of the rate constant was substantially influenced by using a multirotamer treatment. However they were mainly interested in atmospheric chemistry at a temperature of 298 K, and they neglected torsional anharmonicity.

In the present article we consider temperatures up to 2400 K, where torsional anharmonicity can be very important, and we include both multiple-structure anharmonicity and torsional anharmonicity in calculations of partition functions. We report standard state thermochemical properties (for an ideal gas at 1 bar) for the reactant, product, and transition state of the 1,5-hydrogen shift isomerization reaction of the 1-butoxyl radical. The calculated thermochemical properties will be compared to those obtained by the group additivity (GA) method.[11] Multi-structural canonical variational transition state theory including a multidimensional treatment of tunneling (MS-CVT/MT)[12] will be used to obtain accurate forward and reverse rate constants of this reaction in the high-pressure limit.

2. Computational methods

2.1. Electronic structure calculations

The M08-SO[13] density functional combined with the MG3S[14] basis set (which is the same as the 6-311+G(2df,2p) basis set for H, C, and O) has been shown to be a very accurate combination of density functional and basis set for estimation of barrier heights and reaction energies of hydrogen-atom transfer reactions,[15] and this combination has also been shown to perform well for predicting transition state structures.[16] The validity of the M08-SO/MG3S method for the present reaction was examined in a previous study,[4f] in which the best estimate of the classical barrier height (obtained by the CCSD(T)/CBS method) was 11.89 kcal mol^{-1}, and M08-SO/MG3S was shown to yield 12.15 kcal mol^{-1}. Therefore, we will use M08-SO/MG3S for all electronic structure calculations in the present work, in particular, for conformer searching and optimization and for energy and frequency calculations. A locally modified version, *MN-GFM5.0*,[17a] of *Gaussian09.a02*[17b] that contains additional Minnesota functionals is used. The grid for density functional integrations has 99 radial shells around each atom and 974 angular points in each shell.

All vibrational frequencies were scaled by a factor of 0.983, determined previously,[18] to yield a more accurate zero point energy (ZPE). Including the resulting ZPE in the barrier height calculated with the lowest-energy structures of the reactant (or product) and transition state yields 10.72 kcal mol^{-1} for the forward reaction and 14.82 kcal mol^{-1} for the reverse reaction.

2.2. Dynamics calculations

2.2.1. MS-CVT/MT theory. The MS-CVT/MT method has been described in ref. 12. Calculations employing this method begin with the well-known[5] single-structure (SS)

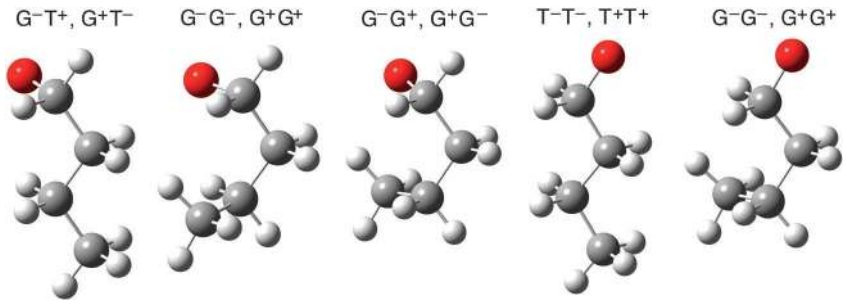

Fig. 1 All conformers of the 1-butoxyl radical. Conformations are depicted here in the order of increasing zero-point-exclusive M08-SO/MG3S energy.

Published on 16 January 2012 on http://pubs.rsc.org | doi:10.1039/C2CP23692C
Downloaded by University of Minnesota - Twin Cities on 04 March 2012

canonical variational transition state theory including multi-dimensional treatment of tunneling (CVT/MT). Then one adds vibrational anharmonicity (multiple-structures and torsional anharmonicity) to the rate constant calculations by multiplying with a multi-structural torsional factor $F^{\text{MS-T}}$. In this way the MS-CVT/MT rate constant is expressed as

$$k^{\text{MS-CVT/MT}} = F^{\text{MS-T}}(T)\kappa^{\text{MT}}(T)k^{\text{CVT}}(T) \qquad (1)$$

where k^{CVT} in eqn (1) is the single-structure CVT rate constant,[5a,19] which minimizes the calculated generalized transition state (GT) rate constant (k^{GT}) for each temperature. For a unimolecular reaction, this is given in the harmonic oscillator (HO) approximation by

$$k^{\text{CVT}} = \min_s k^{\text{GT}}(T,s) = \frac{1}{\beta h}\frac{Q^{\text{GT}}_{\text{el}}(T)Q^{\text{GT}}_{\text{rovib}}(T,s^{\text{CVT}}_*)}{Q^{\text{R}}_{\text{el}}(T)Q^{\text{R}}_{\text{rovib}}(T)}\exp(-\beta V_{\text{MEP}}(s^{\text{CVT}}_*)) \qquad (2)$$

where β is $(k_{\text{B}}T)^{-1}$, k_{B} is Boltzmann's constant, h is Planck's constant, s is the signed distance along the minimum energy path (MEP), s^{CVT}_* is the value of s that minimizes the rate constant, $Q^{\text{GT}}_{\text{el}}$ and $Q^{\text{GT}}_{\text{rovib}}$ are, respectively, the electronic and rotational–vibrational partition functions of the generalized transition state, Q^{R}_{el} and $Q^{\text{R}}_{\text{rovib}}$ are the electronic and rotational–vibrational partition functions of the reactant, and $V_{\text{MEP}}(s^{\text{CVT}}_*)$ is the potential energy at $s = s^{\text{CVT}}_*$. All symmetry numbers for rotations are included in rotational partition functions.

The factor κ^{MT} in eqn (1) is the transmission coefficient, which corrects for quantum effects (tunneling and nonclassical reflection) on the reaction coordinate. In MS-VTST, we assume that the transmission coefficient is the ground-state transmission coefficient taken as the ratio of the thermally averaged ground-state quantal transmission probability to the thermally averaged ground-state classical transmission probability,[20] where "ground-state" here refers to vibrational and rotational modes transverse to the reaction coordinate. The ground-state vibrationally adiabatic potential curve, V^{G}_{a}, governs the tunneling motion,

$$V^{\text{G}}_{\text{a}} = V_{\text{MEP}}(s) + \varepsilon^{\text{G}}(s) \qquad (3)$$

where $\varepsilon^{\text{G}}(s)$ denotes the local zero-point vibrational energy of the bound modes transverse to the reaction coordinate at s. Because ε^{G} depends on s, it means that we already include one effect of the nonseparability of the reaction coordinate in the quantal treatment; thus tunneling calculations based on eqn (3) are labeled as multidimensional. In the present work, we will consider two multidimensional tunneling approximations: zero-curvature tunneling (ZCT)[21] and small-curvature tunneling (SCT).[6] Therefore, MT is either ZCT or SCT.

The product of κ^{MT} and k^{CVT} is called the SS-HO CVT/MT rate constant (where HO denotes harmonic because in eqn (2), $Q^{\text{R}}_{\text{rovib}}$ and $Q^{\text{GT}}_{\text{rovib}}$ are taken as a product of a rotational partition function and a vibrational one that can be calculated using the harmonic formalism (strictly speaking it is quasiharmonic because the scale factor described in Section 2.1 accounts approximately for nontorsional anharmonicity)). This single-structure harmonic approximation is reasonable if neither the generalized TS nor the reactant includes any torsional motion and if they both have only one conformer. However, in most cases we have to consider torsional anharmonicity and multiple-structure anharmonicity in partition functions, and this may have an important influence on the final computed rate constants. There are many methods for correcting harmonic partition functions, such as applying a one-dimensional (1-D) hindered-rotor (HR) approximation[22] to each torsional mode separately and more complicated methods including mode–mode coupling in the treatment of anharmonicity, for example, Feynman path integral methods[23] and the Pitzer–Gwinn approximation.[22a,24] MS-CVT/MT includes anharmonicity by multiplying by a multi-structural torsional factor $F^{\text{MS-T}}$ as shown in eqn (1); this factor is calculated by the multi-structural method for torsional anharmonicity, which is specifically designed for systems with multiple conformers and with multiple torsions coupled with each other and/or with other low-frequency vibrational modes. The MS-T method[10] uses internal-coordinate correction factors to the harmonic treatment, and it avoids assigning specific normal modes as separable torsions. For the present MS-T calculations, we included all structures (AS). The full name of the AS version of the MS-T method is MS-AS-T, but here we shorten it to MS-T.

The first step in using MS-T methods is to find all conformers generated by internal rotations or ring structure isomerizations for both the reactant and the transition state. Since we will also calculate the reverse rate constants, we also consider the product. Then one calculates the corresponding MS-T conformational–rotational–vibrational partition functions *via*

$$Q^{\text{MS-T}}_{\text{con-rovib}} = \sum_{j=1}^{J} Q^{\text{rot}}_j \exp(-\beta U_j) Q^{\text{HO}}_j Z_j \prod_{\tau=1}^{t} f_{j,\tau} \qquad (4)$$

where j labels the distinguishable structures of the investigated species (reactant, product, or transition state), J is the total number of structures, U_j denotes the potential energy of structure j relative to the lowest-potential-energy structure in

 This journal is © the Owner Societies 2012

Published on 16 January 2012 on http://pubs.rsc.org | doi:10.1039/C2CP23692C
Downloaded by University of Minnesota - Twin Cities on 04 March 2012

the relevant set, which is always numbered as $j = 1$, with $U_1 = 0$ by definition, Q_j^{rot} is the classical rotational partition function of structure j, Q_j^{HO} is the usual normal-mode local-harmonic-oscillator vibrational partition function calculated at structure j, Z_j is a factor for guiding the MS-T scheme to the correct high-temperature limit (within the parameters of the model), and $f_{j,\tau}$ is a torsional anharmonicity function, based on internal coordinates, that, in conjunction with Z_j, adjusts the harmonic partition function of structure j in the presence of the torsional motion τ.

For each species, we define the ratio of the calculated MS-T conformational–rotational–vibrational partition function $Q^{\text{MS-T}}_{\text{con-rovib}}$ to $Q^{\text{SS-HO}}_{\text{rovib,1}}$, which is a single-structure harmonic rotational–vibrational partition function of the lowest-potential-energy structure 1, as the MS-T anharmonic factor $F^{\alpha}_{\text{MS-T}}$ of that species (α is either a reactant or product or TS):

$$F^{\alpha}_{\text{MS-T}} = \frac{Q^{\text{MS-T}}_{\text{con-rovib},\alpha}(T)}{Q^{\text{SS-HO}}_{\text{rovib,1},\alpha}(T)} \tag{5}$$

The multi-structural torsional factor $F^{\text{MS-T}}$ in eqn (1) is then obtained as the ratio of $F^{\alpha}_{\text{MS-T}}$ factors of the transition state and reactant. We therefore obtain

$$F^{\text{MS-T}} = \frac{F^{\text{TS}}_{\text{MS-T}}(T)}{F^{\text{R}}_{\text{MS-T}}(T)} \tag{6}$$

The MS-T anharmonic factors of eqn (5) and (6) introduce both multiple-structure and torsional anharmonicity effects. We can decompose the ratios of eqn (5) into a multiple-structure, local-harmonic component $F^{\alpha}_{\text{MS-LH}}$ and a torsional component F^{α}_{T} to clarify their respective contributions,

$$\begin{aligned} F^{\alpha}_{\text{MS-T}} &= F^{\alpha}_{\text{MS-LH}}(T)F^{\alpha}_{\text{T}}(T) \\ &= \left(\frac{Q^{\text{MS-LH}}_{\text{con-rovib},\alpha}(T)}{Q^{\text{SS-HO}}_{\text{rovib,1},\alpha}(T)}\right)\left(\frac{Q^{\text{MS-T}}_{\text{con-rovib},\alpha}(T)}{Q^{\text{MS-LH}}_{\text{con-rovib},\alpha}(T)}\right) \end{aligned} \tag{7}$$

where $Q^{\text{MS-LH}}_{\text{con-rovib},\alpha}(T)$ is the multiple-structure local-harmonic partition function obtained by setting all of the Z_j and $f_{j,\tau}$ equal to unity in eqn (4); this includes anharmonicity from the multiple structures but treats torsions in the vicinity of each local minimum as harmonic oscillators with infinitely high barriers between the structures. (As already mentioned in conjunction with the SS-HO approximation, the MS-LH method is actually quasiharmonic, not strictly harmonic, because of the frequency scaling factors.)

2.2.2. Thermodynamic calculations with the MS-T method. The thermodynamic quantities for one mole of an ideal gas at a standard state pressure of one bar, the Gibbs free energy (G°_T), average energy (E°_T), enthalpy (H°_T), entropy (S°_T), and heat capacity at constant pressure ($C^{\circ}_P(T)$), can be calculated as

$$G^{\circ}_T = -\frac{\ln Q}{\beta} + k_{\text{B}}T \tag{8}$$

$$E^{\circ}_T = -\frac{\partial \ln Q}{\partial \beta} \tag{9}$$

$$H^{\circ}_T = E^{\circ}_T + P^{\circ}V = E^{\circ}_T + RT \tag{10}$$

$$S^{\circ}_T = k_{\text{B}} \ln Q - \frac{1}{T}\left(\frac{\partial \ln Q}{\partial \beta}\right) \tag{11}$$

$$C^{\circ}_P(T) = \left(\frac{\partial H^{\circ}_T}{\partial T}\right)_P \tag{12}$$

where P is the pressure, V is the volume, the little circle denotes the standard state, and Q is the total partition functions including translational, electronic and conformational–vibrational–rotational contributions.

2.2.3. Computational details. Four main steps were carried out to calculate thermochemical properties with the MS-T method and MS-CVT/MT forward and reverse reaction rate constants with potential energy surfaces calculated by the M08-SO/MG3S method:

(1) We performed an exhaustive search for all conformational structures (local minima of the potential energy) of the reactant and product and for all saddle point structures of the transition state. We calculated the ideal-gas partition functions, entropy, heat capacity, enthalpy, and Gibbs free energy for the standard state (1 bar pressure), and we calculated $F^{\alpha}_{\text{MS-T}}$ factors using all generated conformers by the *MSTor* program.[25] The multi-structural torsional factor $F^{\text{MS-T}}$ was calculated using eqn (6).

(2) For each conformer λ of the transition state (λ = 1, 2,. . .,C), we calculate a ground-state energy by

$$V^{\text{G}}_{a,\lambda} = V^{\text{TS}}_{\lambda} + \varepsilon^{\text{G,TS}}_{\lambda} \tag{13}$$

where V^{TS}_{λ} is the potential energy relative to that of the lowest-energy structure of the reactant, and $\varepsilon^{\text{G,TS}}_{\lambda}$ is the zero point energy. Then we used the transition state structure with the lowest $V^{\text{G}}_{a,\lambda}$ and the reactant and product well structures connected to this transition state by its MEP to construct V_{MEP} and V^{G}_{a} curves by the multi-configuration Shepard interpolation method MCSI[26] using the *MCSI* program.[27]

(3) Based on the generated V_{MEP} and V^{G}_{a} curves in step 2, we calculated κ^{MT} and k^{CVT} in eqn (1) for the temperature range 200–2400 K by using the *MC-TINKERATE* program.[28] The global-minimum structures of the reactant and the transition state were used to calculate SS-HO partition functions in calculation of k^{CVT} with eqn (2).

(4) The forward rate constants $k^{\text{MS-CVT/MT}}$ over the 200–2400 K range were obtained using eqn (1). The corresponding $k^{\text{MS-CVT/MT}}$ reverse rate constants were calculated by using the partition function of the product instead of that of the reactant.

In the MCSI calculations of the potential energy surface and vibrationally adiabatic potential energy curve (steps 2 and 3 above), we used the energies, gradients, and Hessians of the saddle point, well structures in the reactant and product valleys, and 18 nonstationary points close to the MEP; these data were calculated by the M08-SO/MG3S method, and these 21 points will be labeled as Shepard points. The potential energy surface was then created by multi-configuration Shepard interpolation using these data. The locations of the first six nonstationary Shepard points were obtained in a similar way to that presented in a previous paper,[26b] and the other 12 non-stationary Shepard points were added for smoothing the V^{G}_{a} curve. Ten of the 18 non-stationary Shepard points were located on the 1-butoxyl side of the saddle point with energies 0.31, 0.62, 1.60, 2.28, 3.25, 4.73, 6.23, 7.77, 9.41, and 9.76 kcal mol^{-1} below the transition state; and the other eight were located on

Published on 16 January 2012 on http://pubs.rsc.org | doi:10.1039/C2CP23692C
Downloaded by University of Minnesota - Twin Cities on 04 March 2012

the 4-hydroxy-1-butyl side with energies 0.89, 1.54, 2.99, 4.60, 6.07, 6.26, 7.69, and 9.48 kcal mol^{-1} below the transition state. The Euler steepest-descents integrator (ESD) was used with a step size of 0.0053 Å to follow the MEP, and the RODS[29] algorithm was used to refine the energies and frequencies along the path. The parameters for the molecular mechanics force field used in the MCSI calculations are those of the modified MM3 force field,[30] and the modified parameters are given in ESI.†

In all calculations of partition functions and the V_a^G curve, the harmonic frequencies obtained from M08-SO/MG3S electronic structure calculations were scaled by an empirical factor of 0.983[18] to reduce the average error in zero-point energies calculated by the local harmonic approximation. The use of the scaling factor introduces anharmonicity into the low-temperature results.

3. Results and discussion

3.1. Conformers, partition functions, and anharmonicity of stationary points (reactant, product, and transition state)

Information about the conformers of the reactant (1-butoxyl) and product (4-hydroxy-1-butyl) and their partition functions and MS-T factors is presented in Tables 1–5. There are ten distinguishable structures (five pairs of mirror images) for the 1-butoxyl radical and 37 distinguishable structures (18 pairs of mirror images plus one symmetric structure with a mirror plane) for the 4-hydroxy-1-butyl radical. The five lowest-energy structures of reactant and product are shown in Fig. 1 and 2.

3.1.1. 1-Butoxyl. As stated in the Introduction, nine distinguishable structures generated by two torsions (O–C–C–C and C–C–C–C) were expected for 1-butoxyl, but we found ten. The naming convention for labeling the structures is given in Table 1. The lowest-energy structures are G^-T^+ and G^+T^-, which are a pair of mirror images.

In the present investigations with the M08-SO density functional, the all-*trans* symmetric structure TT expected originally splits into two mirror images T^-T^- and T^+T^+ with similar geometries, and in particular the two torsion angles are ±178.1° and ±179.3° respectively. The two minima correspond to almost the same geometry on the potential energy surface. We considered including only one of them in the MS-T partition function calculations, using nine structures instead of ten, and this gives results differing from those obtained using all ten structures by 17% at 200 K, 11% at 1000 K, 7% at 1500 K, and 5% at 2400 K (the *M* value for the T^-T^- structure is 4.25 for ten structures and 3.04 for nine). But all structures are present, so in the final calculations we used all ten.

Table 1 Naming convention and labeling of structures

Naming convention	Abbreviation	Dihedral angle range/°
trans	T	180
trans±	$T^{\pm}$	(±150, ±180)
anti±	$A^{\pm}$	(±105, ±150)
	$a^{\pm}$	(±90, ±105)
gauche±	$g^{\pm}$	(±75, ±90)
	$G^{\pm}$	(±30, ±75)
cis±	$C^{\pm}$	(±0, ±30)
cis	C	0

Table 2 Names of structures and their relative conformational energies (in kcal mol^{-1})

Structures	Relative conformational M08-SO[c] energy	
	Zero-point-exclusive	Zero-point-inclusive
1-Butoxyl[a]		
G^-T^+, G^+T^-	0.00	0.00
G^-G^-, G^+G^+	0.17	0.54
g^-G^+, g^+G^-	0.22	0.71
T^-T^-, T^+T^+	0.44	0.28
T^-G^-, T^+G^+	0.69	1.02
4-Hydroxy-1-butyl[b]		
$G^-G^+G^-T^+$, $G^+G^-G^+T^-$	0.00	0.00
$G^-G^+G^+T^-$, $G^+G^-G^-T^+$	0.41	0.30
$T^+G^-G^-T^+$, $T^-G^+G^+T^-$	0.43	0.14
$G^-G^-G^-T^+$, $G^+G^+G^+T^-$	0.77	0.43
$T^+G^-T^+$ T^+, $T^-G^+T^-T^-$	0.79	0.37
$T^+G^-T^-T^-$, $T^-G^+T^+T^+$	0.81	0.32
$G^-G^-T^+T^-$, $G^+G^+T^-T^+$	0.92	0.45
$G^-G^-T^+T^+$, $G^+G^+T^-T^-$	0.92	0.46
$T^+T^-G^+T^-$, $T^-T^+G^-T^+$	0.98	0.58
$G^-T^-G^+T^-$, $G^+T^+G^-T^+$	1.09	0.72
$G^-T^-G^-T^+$, $G^+T^+G^+T^-$	1.13	0.73
$G^-G^+T^+T^-$, $G^+G^-T^-T^+$	1.17	0.75
$G^-G^+T^+T^+$, $G^+G^-T^-T^-$	1.20	0.72
$G^-T^-T^+T^+$, $G^+T^+T^-T^-$	1.32	0.83
$T^+T^+T^-T^-$, $T^-T^-T^+T^+$	1.35	0.69
$G^+T^+T^+T^+$, $G^-T^-T^-T^-$	1.35	0.80
$G^-G^-g^+G^+$, $G^+G^+g^-G^-$	1.61	1.19
$TTTg^+$, $TTTg^-$[d]	1.71	1.31
$T^+G^-g^+T^+$, $T^-G^+g^-T^-$	1.92	1.57

[a] First torsion angle in the structure abbreviations for 1-butoxyl indicates the O–C–C–C angle, while the second indicates the C–C–C–C angle. [b] First torsion angle in the structure abbreviations for 4-hydroxy-1-butyl indicates the H–O–C–C angle, the second indicates the O–C–C–C angle, the third is the C–C–C–C torsion angle, and the fourth is the C–C–C–H torsion. [c] The basis set used for M08-SO is MG3S. [d] The two mirror images are indistinguishable structures, and they will be accounted as one structure in calculations of partition functions.

The energy difference between the lowest and highest of the ten structures is very small, less than 0.69 (or 1.02) kcal mol^{-1} when zero-point energy is excluded (or included); hence the conformational–rotational–vibrational partition functions considering all ten structures ($Q_{\text{con-rovib}}^{\text{MS-LH}}$, $Q_{\text{con-rovib}}^{\text{MS-T}}$) are much larger than the single-structure rotational–vibrational partition functions calculated with the lowest-energy structure ($Q_{\text{rovib,1}}^{\text{SS-HO}}$) as shown in Table 3. The multi-structural torsional factors $F_{\text{MS-T}}^{\text{R}}$ and their components $F_{\text{MS-LH}}^{\text{R}}$ and F_{T}^{R} of 1-butoxyl calculated with eqn (7) are shown in Table 5. They indicate that both multiple-structure and torsional anharmonicity increase the partition functions of 1-butoxyl except for at temperature 2400 K where torsional anharmonicity very slightly decreases the partition functions, and the final MS-T conformational–rotational–vibrational partition functions $Q_{\text{con-rovib}}^{\text{MS-T}}$ are as much as 4.98–11.46 times larger than $Q_{\text{rovib,1}}^{\text{SS-HO}}$ over the 200–2400 K temperature range. The $F_{\text{MS-LH}}^{\text{R}}$ factor is larger than F_{T}^{R} at each temperature studied here.

3.1.2. 4-Hydroxy-1-butyl. The four torsions of the product, 4-hydroxy-1-butyl, are H–O–C–C, O–C–C–C, C–C–C–C, and C–C–C–H, and they generate 37 low-energy distinguishable

 This journal is © the Owner Societies 2012

Published on 16 January 2012 on http://pubs.rsc.org | doi:10.1039/C2CP23692C
Downloaded by University of Minnesota - Twin Cities on 04 March 2012

Table 3 Calculated total partition functions with the multi-structural method, conformational–rotational–vibrational partition function of the 1-butoxyl radical, and the single-structure harmonic rotational–vibrational partition function of the lowest-energy structure of the 1-butoxyl radical[a]

T/K	$Q^{\text{MS-LH}}$	$Q^{\text{MS-T}}$	$Q^{\text{MS-LH}}_{\text{con-rovib}}$	$Q^{\text{MS-T}}_{\text{con-rovib}}$	$Q^{\text{SS-HO}}_{\text{rovib,1}}$
200	1.12×10^{-68}	1.32×10^{-68}	6.12×10^{-76}	7.21×10^{-76}	1.45×10^{-76}
250	1.18×10^{-51}	1.46×10^{-51}	3.68×10^{-59}	4.55×10^{-59}	7.63×10^{-60}
298.15	1.67×10^{-40}	2.15×10^{-40}	3.36×10^{-48}	4.33×10^{-48}	6.35×10^{-49}
300	3.83×10^{-40}	4.94×10^{-40}	7.58×10^{-48}	9.78×10^{-48}	1.43×10^{-48}
400	2.07×10^{-25}	2.88×10^{-25}	2.00×10^{-33}	2.78×10^{-33}	3.32×10^{-34}
600	8.15×10^{-10}	1.23×10^{-09}	2.85×10^{-18}	4.30×10^{-18}	4.15×10^{-19}
800	3.15×10^{-01}	4.83×10^{-01}	5.36×10^{-10}	8.22×10^{-10}	7.30×10^{-11}
1000	$1.65 \times 10^{+05}$	$2.46 \times 10^{+05}$	1.60×10^{-04}	2.39×10^{-04}	2.09×10^{-05}
1500	$1.77 \times 10^{+14}$	$2.32 \times 10^{+14}$	$6.09 \times 10^{+04}$	$7.98 \times 10^{+04}$	$7.55 \times 10^{+03}$
2000	$1.01 \times 10^{+20}$	$1.12 \times 10^{+20}$	$1.63 \times 10^{+10}$	$1.81 \times 10^{+10}$	$1.97 \times 10^{+09}$
2400	$3.07 \times 10^{+23}$	$2.97 \times 10^{+23}$	$3.03 \times 10^{+13}$	$2.94 \times 10^{+13}$	$3.61 \times 10^{+12}$

[a] Geometries, energies, and frequencies were calculated by the M08-SO/MG3S method. The zero of energy for the partition function calculations is the lowest-energy classical equilibrium structure energy (G^-T^+ which is the same as the G^+T^- energy).

Table 4 Calculated total partition functions with the multi-structural method, the conformational–rotational–vibrational partition function of the 4-hydroxy-1-butyl radical, and the single structure harmonic rotational–vibrational partition function of the lowest-energy structure of the 4-hydroxy-1-butyl radical[a]

T/K	$Q^{\text{MS-LH}}$	$Q^{\text{MS-T}}$	$Q^{\text{MS-LH}}_{\text{con-rovib}}$	$Q^{\text{MS-T}}_{\text{con-rovib}}$	$Q^{\text{SS-HO}}_{\text{rovib,1}}$
200	1.02×10^{-68}	1.38×10^{-68}	5.64×10^{-76}	7.65×10^{-76}	2.51×10^{-77}
250	1.79×10^{-51}	2.44×10^{-51}	5.65×10^{-59}	7.71×10^{-59}	1.74×10^{-60}
298.15	3.64×10^{-40}	4.92×10^{-40}	7.41×10^{-48}	1.00×10^{-47}	1.74×10^{-49}
300	8.44×10^{-40}	1.14×10^{-39}	1.69×10^{-47}	2.29×10^{-47}	3.94×10^{-49}
400	7.73×10^{-25}	9.99×10^{-25}	7.55×10^{-33}	9.76×10^{-33}	1.20×10^{-34}
600	5.64×10^{-09}	6.39×10^{-09}	2.00×10^{-17}	2.27×10^{-17}	2.06×10^{-19}
800	$3.11 \times 10^{+00}$	$3.04 \times 10^{+00}$	5.37×10^{-09}	5.24×10^{-09}	4.37×10^{-11}
1000	$2.03 \times 10^{+06}$	$1.71 \times 10^{+06}$	2.00×10^{-03}	1.69×10^{-03}	1.41×10^{-05}
1500	$2.89 \times 10^{+15}$	$1.71 \times 10^{+15}$	$1.04 \times 10^{+06}$	$6.14 \times 10^{+05}$	$5.99 \times 10^{+03}$
2000	$1.84 \times 10^{+21}$	$7.95 \times 10^{+20}$	$3.21 \times 10^{+11}$	$1.39 \times 10^{+11}$	$1.67 \times 10^{+09}$
2400	$5.77 \times 10^{+24}$	$2.00 \times 10^{+24}$	$6.39 \times 10^{+14}$	$2.21 \times 10^{+14}$	$3.17 \times 10^{+12}$

[a] Geometries, energies, and frequencies were calculated by the M08-SO/MG3S method. The zero of energy for the partition function calculations is the lowest-energy classical equilibrium structure energy ($G^-G^+G^-T^+$ which is the same as the $G^+G^-G^+T^-$ energy).

Table 5 Multi-structural torsional factors of 1-butoxyl and 4-hydroxy-1-butyl

	1-Butoxyl			4-Hydroxy-1-butyl		
T/K	$F^{\text{R}}_{\text{MS-T}}$	$F^{\text{R}}_{\text{MS-LH}}$	F^{R}_{T}	$F^{\text{P}}_{\text{MS-T}}$	$F^{\text{P}}_{\text{MS-LH}}$	F^{P}_{T}
200	4.98	4.23	1.18	30.44	22.46	1.36
250	5.96	4.83	1.24	44.38	32.53	1.36
298.15	6.82	5.29	1.29	57.54	42.54	1.35
300	6.85	5.31	1.29	58.03	42.94	1.35
400	8.36	6.02	1.39	81.61	63.17	1.29
600	10.35	6.87	1.51	110.16	97.23	1.13
800	11.26	7.34	1.53	119.92	122.71	0.98
1000	11.46	7.65	1.50	119.46	141.90	0.84
1500	10.58	8.07	1.31	102.54	173.12	0.59
2000	9.19	8.29	1.11	82.97	191.52	0.43
2400	8.13	8.40	0.97	69.73	201.51	0.35

structures (18 pairs of mirror images plus one symmetric structure with a mirror plane). These structures have very similar energies; in particular the energy differences between the 37 structures are smaller than 1.92 (or 1.57) kcal mol^{-1} when zero-point-energy is excluded (or included). The lowest-energy structures are $G^-G^+G^-T^+$ and $G^+G^-G^+T^-$, which are 1.35 kcal mol^{-1} lower in energy than the all *trans* structure that was sometimes taken as the lowest-energy structure in previous work.

As a result of a large number of conformers, multi-structural torsional anharmonicity, especially anharmonicity introduced by multiple structures, has a remarkable effect on the partition functions of the 4-hydroxy-1-butyl radical as shown in Table 4. The $F^{\text{P}}_{\text{MS-T}}$ given in Table 5 are as large as 30.4–119.9 over the temperature range 200–2400 K, while $F^{\text{P}}_{\text{MS-LH}}$ are as large as 22.5–201.5. Due to the mode–mode coupling, the torsional anharmonicity at temperatures higher than 800 K has a negative effect on partition functions; thus it leads to F^{P}_{T} values smaller than unity.

3.1.3. Transition state. The transition state of the 1,5-H shift reaction of 1-butoxyl is a six-membered ring structure without torsions; therefore, only two distinguishable structures (one pair of mirror images) were located in the present work, and these are shown in Fig. 3. Thus, for the transition state, there is no torsional anharmonicity, and $Q^{\text{MS-LH}}_{\text{con-rovib,TS}}$ are exactly equal to $Q^{\text{MS-T}}_{\text{con-rovib,TS}}$, which is twice as large as the SS-HO rotational–vibrational partition function for each temperature. The calculated total partition functions $Q^{\text{MS-T}}_{\text{TS}}$ and $Q^{\text{MS-T}}_{\text{con-rovib,TS}}$ of the transition state for temperature 200–2400 K and the multi-structural torsional factors are shown in Table 6. Due to the absence of torsion motion and only two degenerate conformers, F^{TS}_{T} is 1, and $F^{\text{TS}}_{\text{MS-LH}}$ and $F^{\text{TS}}_{\text{MS-T}}$ are equal to each other and have a value of 2 at all temperatures.

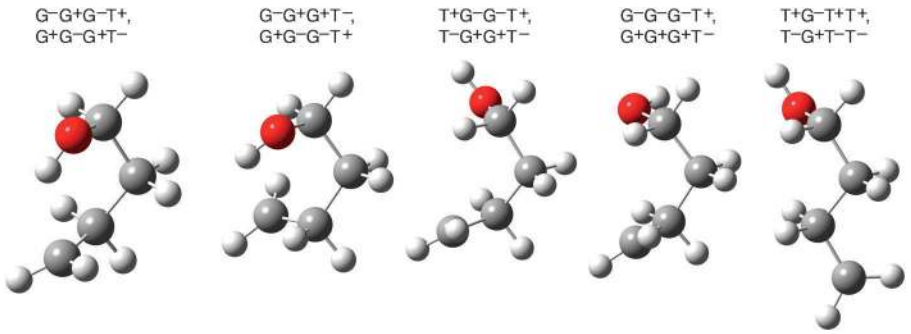

Fig. 2 Five lowest-energy conformations for the 4-hydroxy-1-butyl radical. Conformations are depicted here in the order of increasing zero-point exclusive M08-SO/MG3S energy.

Published on 16 January 2012 on http://pubs.rsc.org | doi:10.1039/C2CP23692C
Downloaded by University of Minnesota - Twin Cities on 04 March 2012

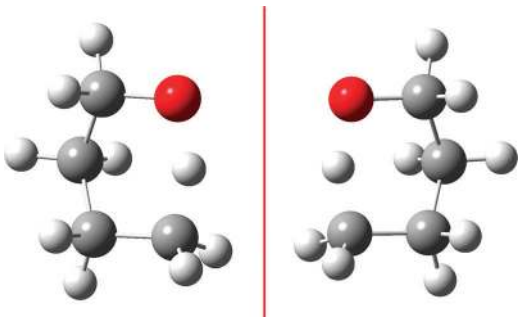

Fig. 3 Two distinguishable structures (TS1, TS2) of the transition state.

Table 6 Calculated total partition functions and conformational–rotational–vibrational partition functions with the multi-structural torsional method and multi-structural torsional factors of the transition state[a]

T/K	$Q^{\text{MS-T}}$	$Q^{\text{MS-T}}_{\text{con-rovib,TS}}$	$F^{\text{TS}}_{\text{MS-T}}$	$F^{\text{TS}}_{\text{MS-LH}}$	F^{TS}_{T}
200	1.47×10^{-67}	7.99×10^{-75}	2	2	1
250	3.91×10^{-51}	1.22×10^{-58}	2	2	1
298.15	2.16×10^{-40}	4.35×10^{-48}	2	2	1
300	4.80×10^{-40}	9.50×10^{-48}	2	2	1
400	7.08×10^{-26}	6.82×10^{-34}	2	2	1
600	6.75×10^{-11}	2.36×10^{-19}	2	2	1
800	1.22×10^{-02}	2.07×10^{-11}	2	2	1
1000	$3.91 \times 10^{+03}$	3.82×10^{-06}	2	2	1
1500	$2.04 \times 10^{+12}$	$7.21 \times 10^{+02}$	2	2	1
2000	$7.44 \times 10^{+17}$	$1.28 \times 10^{+08}$	2	2	1
2400	$1.73 \times 10^{+21}$	$1.89 \times 10^{+11}$	2	2	1

[a] Geometries, energies, and frequencies were calculated by the M08-SO/MG3S method.

3.2 Thermodynamics quantities

As shown in eqn (8)–(12), all the thermodynamics quantities are determined by the total partition functions. The multi-structural torsional anharmonicity which plays an important role in calculations of partition function will directly affect the accuracy of these thermodynamics quantities. Tables 7–9 list the calculated temperature-dependent standard-state (one bar) ideal-gas entropy S°_T, heat capacity $C^{\circ}_P(T)$, relative enthalpy $H^{\circ}_T - H^{\circ}_0$, and relative Gibbs free energy $G^{\circ}_T - H^{\circ}_0$ using multi-structural torsional partition functions for 1-butoxyl, 4-hydroxy-1-butyl, and the transition state that interconnects them. For comparison, those entropy and heat capacity obtained by Benson's group additivity (GA) method[11] are given for 1-butoxyl and 4-hydroxy-1-butyl. The heat capacities obtained by Davis and Francisco[4g] using the G4 method with a single structure are also shown in Tables 7–9.

Table 7 Standard state (1 bar) entropy (in cal mol^{-1} K^{-1}), heat capacity (in cal mol^{-1} K^{-1}), relative enthalpy (in kcal mol^{-1}), and relative Gibbs free energy (in kcal mol^{-}) of ideal gas for the 1-butoxyl radical

	S°_T			$C^{\circ}_P(T)$			
T/K	MS-LH	MS-T	GA[a]	MS-LH	MS-T	GA[a]	Ref. 4g[b]
200	76.12	76.84		19.85	20.57		17.6
250	80.81	81.69		22.41	23.14		
298.15	85.00	86.01	83.85	25.32	25.97		22.7
300	85.16	86.17	84.02	25.44	26.09	25.09	22.8
400	93.38	94.52	92.17	32.00	32.28	31.54	28.6
600	108.61	109.70	107.05	43.37	42.75	42.29	38.6
800	122.29	123.10	121.48	51.71	50.41	50.16	46.1
1000	134.53	134.99	132.67	57.94	56.18	55.85	51.8
1500	160.09	159.69	161.49	67.62	65.26		
2000	180.28	179.16		72.47	69.84		
2400	193.70	192.08		74.63	71.88		

	$H^{\circ}_T - H^{\circ}_0$		$G^{\circ}_T - H^{\circ}_0$	
T/K	MS-LH	MS-T	MS-LH	MS-T
200	2.91	2.99	−12.32	−12.38
250	3.96	4.08	−16.24	−16.35
298.15	5.11	5.26	−20.23	−20.39
300	5.16	5.31	−20.39	−20.54
400	8.03	8.23	−29.32	−29.58
600	15.62	15.78	−49.55	−50.04
800	25.17	25.14	−72.66	−73.34
1000	36.17	35.82	−98.37	−99.17
1500	67.84	66.44	−172.29	−173.10
2000	103.00	100.34	−257.57	−257.97
2400	132.45	128.72	−332.43	−332.28

[a] Using group values from ref. 11, and for entropy, adding 0.026 cal mol^{-1} K^{-1} to convert from a standard pressure of 1 atm to a standard pressure of 1 bar. [b] The data are obtained from ref. 4g, where the single-structure method was used for G4 data set.

The heat capacities calculated with the MS-T method considering both multiple-structure and torsional anharmonicity are in reasonable agreement with those obtained by the GA method for 1-butoxyl and 4-hydroxy-1-butyl. Although for 1-butoxyl, the MS-LH method only considering multiple-structure anharmonicity gives $C^{\circ}_P(T)$ values closer to the GA values for 300 and 400 K, the MS-LH method overestimates the heat capacities at most temperatures for both 1-butoxyl and 4-hydroxy-1-butyl. The heat capacities obtained

This journal is © the Owner Societies 2012

Downloaded by University of Minnesota - Twin Cities on 04 March 2012
Published on 16 January 2012 on http://pubs.rsc.org | doi:10.1039/C2CP23692C

Table 8 Standard state (1 bar) entropy (in cal mol^{-1} K^{-1}), heat capacity (in cal mol^{-1} K^{-1}), relative enthalpy (in kcal mol^{-1}), and relative Gibbs free energy (in kcal mol^{-1}) of ideal gas for the 4-hydroxy-1-butyl radical

	S°_T			$C^{\circ}_P(T)$			
T/K	MS-LH	MS-T	GA[a]	MS-LH	MS-T	GA[a]	Ref. 4g[b]
200	80.76	81.53		21.93	21.34		20.6
250	85.92	86.52		24.445	23.63		
298.15	90.46	90.90	89.94	27.27	26.28		26.3
300	90.63	91.07	90.11	27.39	26.38	26.01	26.4
400	99.34	99.46	98.45	33.66	32.32	31.97	32.7
600	115.15	114.58	113.63	44.36	42.47	42.01	43.5
800	129.03	127.84	126.77	52.09	49.76	49.34	51.3
1000	141.30	139.54	138.83	57.81	55.15	54.77	57.1
1500	166.63	163.67	166.61	66.75	63.58		
2000	186.54	182.60		71.39	67.93		
2400	199.76	195.17		73.56	69.96		

	$H^{\circ}_T - H^{\circ}_0$		$G^{\circ}_T - H^{\circ}_0$	
T/K	MS-LH	MS-T	MS-LH	MS-T
200	3.30	3.34	−12.85	−12.97
250	4.46	4.46	−17.02	−17.18
298.15	5.70	5.66	−21.27	−21.45
300	5.76	5.71	−21.45	−21.62
400	8.81	8.64	−30.95	−31.15
600	16.67	16.18	−52.44	−52.59
800	26.35	25.44	−76.89	−76.86
1000	37.37	35.95	−103.96	−103.61
1500	68.76	65.88	−181.23	−179.67
2000	103.41	98.87	−269.72	−266.39
2400	132.43	126.47	−347.05	−341.99

[a] Using group values from ref. 11, and for entropy, adding 0.026 cal mol^{-1} K^{-1} to convert from a standard pressure of 1 atm to a standard pressure of 1 bar. [b] The data are obtained from ref. 4g, where the single structure method was used for G4 data set.

Table 9 Standard state (1 bar) entropy (in cal mol^{-1} K^{-1}), heat capacity (in cal mol^{-1} K^{-1}), relative enthalpy (in kcal mol^{-1}), and relative Gibbs free energy (in kcal mol^{-1}) of ideal gas calculated by the MS-T method for the transition state

T/K	S°_T	$C^{\circ}_P(T)$[a]	$H^{\circ}_T - H^{\circ}_0$	$G^{\circ}_T - H^{\circ}_0$
200	68.09	15.57/15.2	2.15	−11.47
250	71.91	18.85	3.01	−14.97
298.15	75.52	22.36/21.8	4.00	−18.52
300	75.66	22.50/22.0	4.04	−18.66
400	83.16	29.96/29.3	6.67	−26.60
600	97.77	42.18/41.4	13.96	−44.71
800	111.13	50.62/49.9	23.29	−65.62
1000	123.11	56.64/56.0	34.04	−89.07
1500	148.00	65.61	64.88	−157.11
2000	167.55	70.06	98.92	−236.18
2400	180.52	72.09	127.38	−305.86

[a] The values after slash are from ref. 4g, where the single-structure method was used for G4 data set.

by Davis and Francisco are based on considering only a single structure, and they have a large deviation from those calculated by MS methods in the present work and from the empirical GA results for 1-butoxyl. For 4-hydroxy-1-butyl and the transition state, Davis and Francisco's results are similar to our MS-LH heat capacities.

Similarly, the entropies calculated with MS methods are in reasonable agreement with GA results. Although MS-T entropies have a deviation of 2–3 cal mol^{-1} K^{-1} from the GA entropies at some temperatures, the MS-T results may be more reliable than the empirical GA values and the MS-LH results.

Table 10 The calculated multi-structural torsional factors for rate calculations of forward reaction and reverse reaction

	Forward reaction			Reverse reaction		
T/K	$F^{\text{MS-T}}$	$F^{\text{MS-LH}}$	F^{T}	$F^{\text{MS-T}}$	$F^{\text{MS-LH}}$	F^{T}
200	0.402	0.473	0.849	0.066	0.089	0.738
250	0.336	0.415	0.809	0.045	0.061	0.733
298.15	0.293	0.378	0.776	0.035	0.047	0.739
300	0.292	0.377	0.774	0.034	0.047	0.740
400	0.239	0.332	0.720	0.025	0.032	0.774
600	0.193	0.291	0.663	0.018	0.021	0.883
800	0.178	0.272	0.652	0.017	0.016	1.023
1000	0.175	0.262	0.667	0.017	0.014	1.188
1500	0.189	0.248	0.763	0.020	0.012	1.688
2000	0.218	0.241	0.902	0.024	0.010	2.308
2400	0.246	0.238	1.033	0.029	0.010	2.890

3.3. Multi-structural torsional factors and anharmonicity of the reactions

The multi-structural torsional anharmonicity factors ($F^{\text{MS-T}}$, $F^{\text{MS-LH}}$, and F^{T}) for rate calculations of the forward or reverse reaction are obtained using eqn (6) and are shown in Table 10. The smaller number of structures of the transition state as compared to the reactant and product leads to $F^{\text{MS-T}}$ factors being smaller than unity for both the forward and reverse reactions. Therefore the multi-structural torsional anharmonicity reduces the final thermal rate constants. The $F^{\text{MS-T}}$ factor of the forward reaction decreases gradually from 0.40 at 200 K to 0.17 at 1000 K, and then it increases gently to 0.25 at 2400 K. The $F^{\text{MS-T}}$ factors of the reverse reaction are much smaller than those of the forward reaction because there are much more conformers of the product than of the reactant, and they are 0.066, 0.017, and 0.029 for temperatures of 200, 800, and 2400 K. From Table 10, one can notice that multiple-structure anharmonicity has larger effects on partition functions than torsional anharmonicity in the present case.

3.4. CVT/MT rate constants and transmission coefficients

The forward and reverse barrier heights and the reaction energy calculated using the lowest-energy structures of reactant, product, and transition state are 12.59, 17.26, and −4.67 kcal mol^{-1}, respectively, by the M08-SO/MG3S method before including ZPE. The calculated barrier heights are larger than those (12.15 kcal mol^{-1} for forward reaction and 15.92 kcal mol^{-1} for reverse reaction by the M08-SO/MG3S method) in previous work by two of us,[4f] because we now use those more stable conformers of the reactant and product. Table 11 compares the calculated enthalpy of reaction and enthalpy of activation obtained by the MS-T method in the present work with those obtained by Davis and Francisco[4g] using the G4 method and only considering a single structure, and those estimated by the GA method.

The calculated potential energy along the minimum energy path, V_{MEP}, and the ground-state vibrationally adiabatic potential curve, V_{a}^{G}, are shown in Fig. 4. Using these potential curves, the single-structure harmonic (in fact it should be called quasiharmonic because the scaling factor is used in

Downloaded by University of Minnesota - Twin Cities on 04 March 2012
Published on 16 January 2012 on http://pubs.rsc.org | doi:10.1039/C2CP23692C

Table 11 Standard state enthalpy of reaction and enthalpy of activation (kcal mol^{-1})

	Enthalpy of reaction			Enthalpy of activation	
T/K	Present	Ref. 4g[a]	GA[b]	Present	Ref. 4g[a]
Forward reaction					
0	−4.10	−3.4		10.72	10.4
298	−3.70	−3.0	−3.25	9.46	9.5
1000	−3.97	n.a.	−3.35	8.94	n.a.
2000	−5.58	n.a.		9.30	n.a.
Reverse reaction					
0	4.10	3.4		14.82	n.a
298	3.70	3.0	3.25	13.16	n.a.
1000	3.97	n.a.	3.35	12.91	n.a.
2000	5.58	n.a.		14.87	n.a.

[a] Davis and Francisco's single structure G4 method. [b] Using group values from ref. 11.

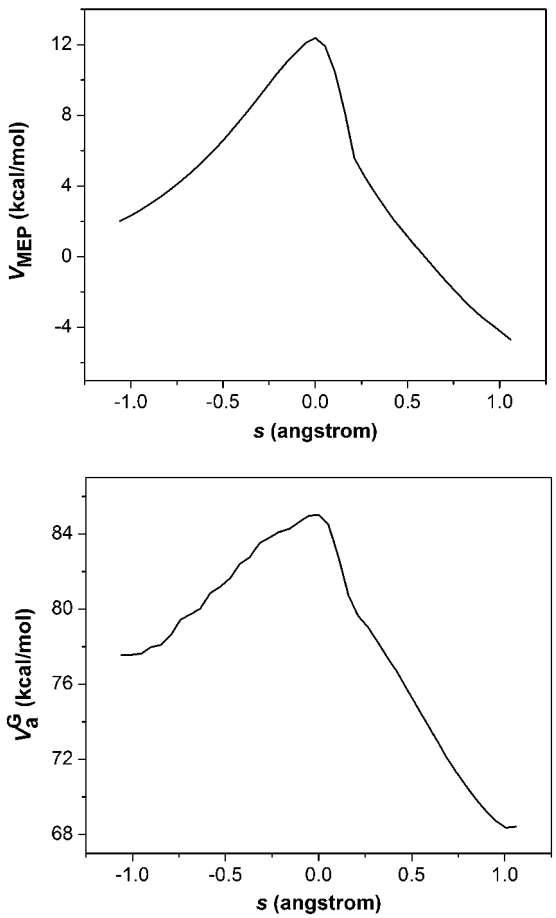

Fig. 4 Calculated potential energy along the minimum energy path (V_{MEP}) and ground-state vibrationally adiabatic potential curve (V_a^G) *vs.* the reaction coordinate s, where the reaction coordinate is scaled to a reduced mass of 1 amu.

the zero point energy calculations) CVT rate constants k^{CVT} and corresponding transmission coefficient κ^{MT} (MT can be ZCT or SCT) for both forward and reverse reactions are evaluated. Fig. 5 plots the common logarithm of the ZCT and SCT transmission coefficients as functions of 1000/T. As we expected, the κ^{ZCT} values are much smaller than the κ^{SCT} ones at low temperatures because ZCT underestimates the tunneling, and the difference between them decreases when the temperature increases.

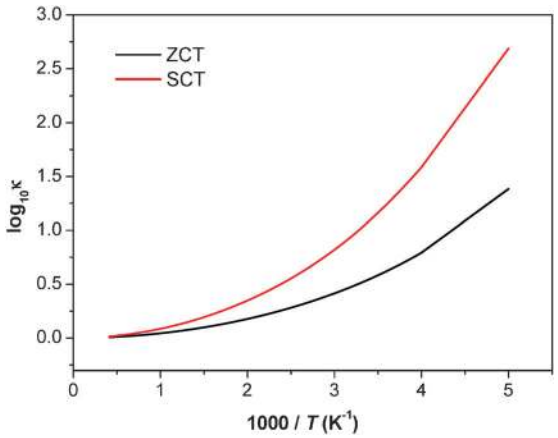

Fig. 5 Calculated common logarithm of the ZCT and SCT transmission coefficients κ *vs.* reciprocal temperature (times a thousand).

The large curvature tunneling (LCT) approximation[31] was not used for this reaction, because we expect that large-curvature tunneling paths would not make a significant contribution for this unimolecular reaction. At T = 300 K, we get κ^{ZCT} = 3.3, and κ^{SCT} = 11.0; both of them are smaller than in the previous work by two of us[4f] where κ^{ZCT} = 5.3 and κ^{SCT} = 40.9, but larger than the transmission coefficient corresponding to Somnitz's estimation[4e] for tunneling, which corresponds to κ = 2.7. Davis and Fransisco[4g] significantly overestimated tunneling (κ = 120) with the parabolic tunneling approximation for the G4 data set, and they underestimated tunneling (κ = 3.5) with the Wigner method. It is seen that the transmission coefficients from the various calculations are very different from each other. Extensive previous validation studies have shown that the SCT approximation is much more reliable than the Wigner method, the parabolic tunneling approximation, or the ZCT approximation. The difference between the two SCT calculations has a different origin, namely that the present V_a^G curve is more accurate than the one in ref. 4f; one should remember that transmission coefficients at room temperature and below are very sensitive to small differences in the effective potentials used for the tunneling calculations.

The present work predicts only a small variational effect with the rate constant ratio of CVT to TST ranging from 0.90 to 0.97. In our previous work[4f] this rate ratio ranged from 0.83 to 0.90. Since the previous work[4f] was based on straight direct dynamics calculations whereas the present work involves the MCSI method, the previous work should be more accurate for the variational effect, but fortunately the difference between the two treatments is less than 8%.

The single-structure $k^{CVT/MT}$ (MT can be ZCT or SCT) rate constants including tunneling are obtained as a product of k^{CVT} and κ^{MT}, and are plotted in Fig. 6 as functions of 1000/T along with k^{CVT} rate constants for forward and reverse reactions. As shown in Fig. 6, the forward reaction has larger rate constants than the reverse reaction. Tunneling increases the reaction rate constants especially at low temperatures.

3.5. MS-CVT/MT rate constants

The above calculations provide the factors needed in eqn (1) to calculate the thermal rate constants: κ, F^{MS-T} and k^{CVT}. Fig. 7 displays the plots of the common logarithms of κ^{SCT}, F^{MS-T},

 This journal is © the Owner Societies 2012

Downloaded by University of Minnesota - Twin Cities on 04 March 2012
Published on 16 January 2012 on http://pubs.rsc.org | doi:10.1039/C2CP23692C

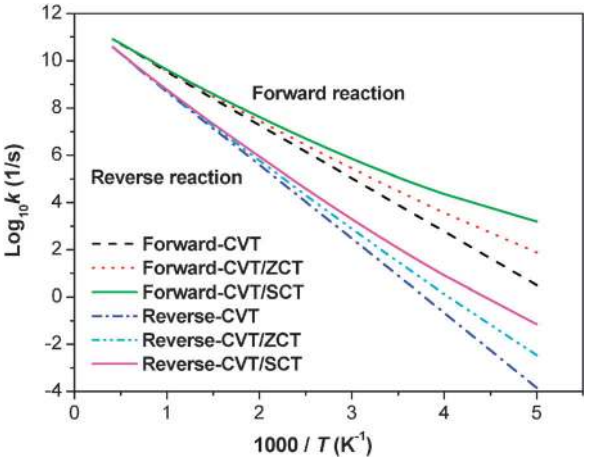

Fig. 6 The temperature dependence of k^{CVT} and $k^{CVT/MT}$ (MT can be ZCT or SCT) rate constants including tunneling for both forward and reverse reactions.

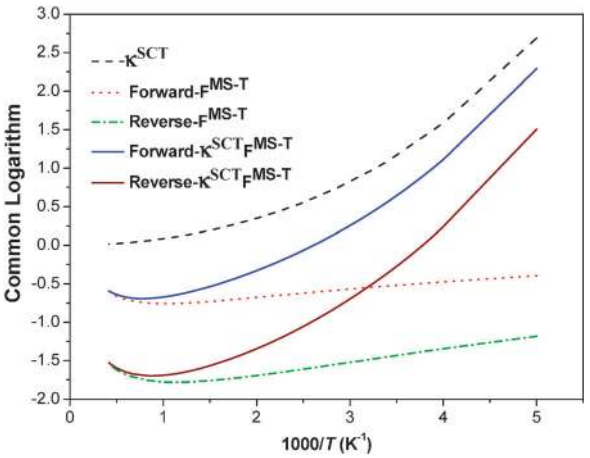

Fig. 7 Common logarithms of κ^{SCT}, of $F^{MS\text{-}T}$, and of their product for the forward and reverse reactions as functions of temperature. Note that κ^{SCT} is the same for the reverse reaction as for the forward one.

and their product for both forward and reverse reactions as a function of temperature, and it shows that the tunneling and anharmonicity effects have opposite effects on the rate constants for the 1,5-hydrogen shift isomerization reaction of 1-butoxyl, and the former increases the rate (positive logarithm), while the latter reduces the rate (negative logarithm). At low temperatures, $T < 385$ K, the tunneling has a larger effect for the forward reaction; at higher temperatures than 385 K, multi-structural torsional anharmonicity has a larger effect on the forward reaction rate. The large number of low-energy conformers of the product has the consequence that the anharmonic effect is larger than the tunneling for the reverse reaction at even lower temperatures ($T > 264$ K). Therefore, both tunneling and multi-structural torsional anharmonicity effects are very important for accurate rate constants calculations if one considers a wide temperature range.

The final $k^{MS\text{-}CVT/MT}$ forward rate constants including these two important effects are obtained using eqn (1), and they are plotted as functions of temperature in Fig. 8. In Fig. 8, the $k^{CVT/SCT}$ rate constants obtained by the single-structure method in the present work and the previous

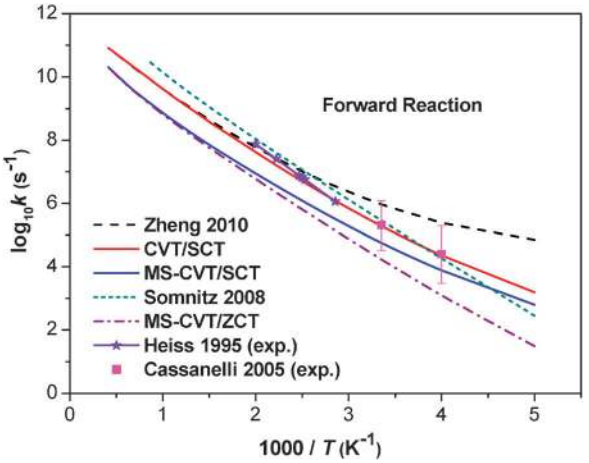

Fig. 8 The calculated $k^{CVT/SCT}$and $k^{MS\text{-}CVT/MT}$ (MT can be ZCT or SCT) forward rate constants compared to previous theoretical[4e,f] and experimental[3b,d] results.

theoretical and experimental results are also given for comparison. The $k^{MS\text{-}CVT/SCT}$ and $k^{CVT/SCT}$ forward rate constants at several temperatures are shown in Table 12. As shown in Fig. 8, the single-structure $k^{CVT/SCT}$ rate constants in the present work agree very well with experimental results of Heiss and Sahetchian[3b] and Cassanelli *et al.*[3d] Due to larger estimated tunneling contributions, the previous single-structure CVT/SCT rate constants obtained by two of us[4f] have a large deviation from the present $k^{CVT/SCT}$ results at low temperature. Another contributing factor to the difference is that we use a more stable reactant structure in the present calculations. Comparison of the present $k^{CVT/SCT}$ rate constants and single-structure rate constants obtained by Somnitz[4e] shows that Somnitz overestimated the rate constants at high temperature and underestimated tunneling at low temperature, but he had rate constants similar to our $k^{CVT/SCT}$ rate constants and Cassanelli *et al.*'s experimental results at 250–300 K. Although these theoretical rate constants by the single-structure method are in good agreement with experimental results, one must realize that these single-structure methods neglect the important multi-structural torsional anharmonicity effects. When multi-structural torsional anharmonicity is considered, the final $k^{MS\text{-}CVT/MT}$ (MT can be either ZCT or SCT) rate constants are much smaller than the ones obtained by single-structure methods. There is a large deviation of the MS-CVT/MT results for the forward reaction from the experimental data, but our smaller $k^{MS\text{-}CVT/SCT}$ results are still located within the error range of Cassanelli *et al.*'s experiments. Due to the underestimation of tunneling by the ZCT method, the $k^{MS\text{-}CVT/ZCT}$ rate constants are much smaller than $k^{MS\text{-}CVT/SCT}$ at low temperatures. As we mentioned in the Introduction, so far all the experimental rate constants reported for the 1-butoxyl isomerization reaction were determined by techniques based on relative rates, and this introduced large uncertainties in the results. Our $k^{MS\text{-}CVT/SCT}$ results include, at a reasonably high level, almost all the factors that could affect the accuracy of rate calculations, and we believe that they are competitive in accuracy with the currently available experimental techniques and may be

Downloaded by University of Minnesota - Twin Cities on 04 March 2012
Published on 16 January 2012 on http://pubs.rsc.org | doi:10.1039/C2CP23692C

Table 12 The $k^{\text{MS-CVT/SCT}}$ and $k^{\text{CVT/SCT}}$ rate constants (s^{-1})

	$k^{\text{MS-CVT/SCT}}$		$k^{\text{CVT/SCT}}$	
T/K	Forward reaction	Reverse reaction	Forward reaction	Reverse reaction
298	$5.66 \times 10^{+04}$[a]	$9.17 \times 10^{+00}$	$1.93 \times 10^{+05}$[a]	$2.64 \times 10^{+02}$
1000	$7.35 \times 10^{+08}$	$9.96 \times 10^{+06}$	$4.21 \times 10^{+09}$	$5.95 \times 10^{+08}$
2000	$1.16 \times 10^{+10}$	$4.95 \times 10^{+08}$	$5.31 \times 10^{+10}$	$2.05 \times 10^{+08}$

[a] The experimental forward reaction rate constant at 298 K is $1.76 \times 10^{+05}$ s^{-1} by Atkinson,[2] $2.0 \times 10^{+05}$ s^{-1} at 1 atm by Cassanelli *et al.*,[3d] and $1.1 \times 10^{+05}$ s^{-1} by Hein *et al.*[3c] after accounting for any pressure fall-off under their experimental conditions (they obtained a rate constant of $(3.5\pm2) \times 10^{+04}$ s^{-1} at 295 ± 3 K and 50 mbar pressure).

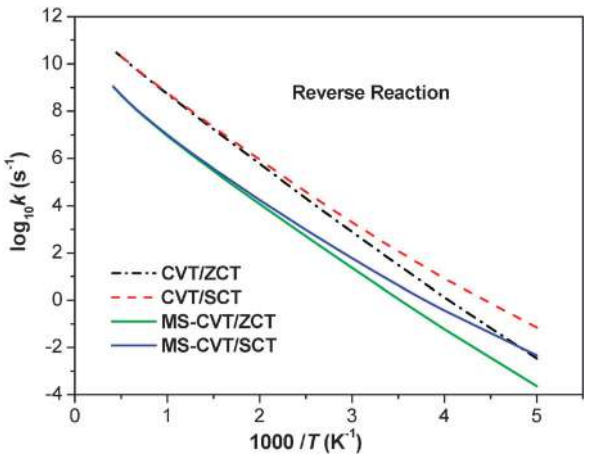

Fig. 9 The calculated $k^{\text{MS-CVT/MT}}$ (MT can be ZCT or SCT) reverse rate constants compared to the corresponding $k^{\text{CVT/MT}}$ rate constant.

more accurate than the currently available experimental rate constants.

As far as we know, neither theoretical nor experimental data for the reverse rate of the 1,5-hydrogen shift isomerization reaction of 1-butoxyl have been reported by other workers. Our investigation of the reverse reaction shows an especially large effect of considering multi-structural torsional anharmonicity, as we discussed in the beginning of this subsection. Fig. 9 shows a large difference between the single-structure and multi-structural rate constants for the reverse reaction.

The calculated $k^{\text{MS-CVT/MT}}$ rate constants for both forward and reverse reactions are fitted to the modified Arrhenius equation[4f]

$$k = A\left(\frac{T}{300}\right)^{n} \exp\left[-\frac{E(T+T_0)}{R(T^2+T_0^2)}\right] \qquad (14)$$

Table 14 E_a (kcal mol^{-1}) calculated by the MS-CVT/SCT method

T/K	Forward reaction	Reverse reaction
200	4.45	8.04
250	5.69	9.45
298.15	6.53	10.30
300	6.56	10.32
400	7.59	11.28
600	8.56	12.25
800	9.18	13.02
1000	9.75	13.82
1500	11.24	15.98
2000	12.84	18.29
2400	14.16	20.21

which has four fitting parameters. The corresponding Arrhenius activation energy is

$$E_a = E\frac{T^4 + 2T_0T^3 - T_0^2T^2}{(T^2+T_0^2)^2} + nRT \qquad (15)$$

The fitted parameters and calculated activation energies for both forward and reverse reactions are listed in Tables 13 and 14. Table 14 shows that the activation energy increases nonlinearly with temperature, which shows clearly that T_0 must be nonzero.

As a result of a different extent of multi-structural torsional anharmonicity for the forward and reverse reactions, the equilibrium constant of the reaction which is the ratio of the forward to reverse rate constants, is also affected by the multi-structural torsional anharmonicity.

4. Concluding remarks

Multi-structural canonical variational transition state theory including a multidimensional treatment of tunneling (MS-CVT/MT) has been applied to the 1,5-hydrogen shift isomerization reaction of 1-butoxyl. The presence of several torsion motions leads to multiple minima (ten and 37) on the potential energy surfaces for both the reactant and product. The mirror image structures of the six-membered ring transition state are included in this work. All conformers of stationary points have been used in calculations of partition functions including multi-structural torsional anharmonicity (we used MS-T conformational–rotational–vibrational partition functions). The thermochemical properties (entropy, heat capacity, relative enthalpy, and relative Gibbs free energies) at a standard state of the reactant 1-butoxyl, the product 4-hydroxy-1-butyl, and their transition state as a 1 bar ideal gas have been calculated using the total MS-T partition functions, and have been compared to those obtained by Benson's group additivity method and by the G4 method that only considers a single structure.

Table 13 The parameters in the fits to $k^{\text{MS-CVT/MT}}$ rate constants, where MT is ZCT or SCT

	Forward reaction		Reverse reaction	
	$k^{\text{MS-CVT/ZCT}}$	$k^{\text{MS-CVT/SCT}}$	$k^{\text{MS-CVT/ZCT}}$	$k^{\text{MS-CVT/SCT}}$
A/s^{-1}	$2.033 \times 10^{+09}$	$1.514 \times 10^{+09}$	$4.737 \times 10^{+07}$	$2.672 \times 10^{+07}$
n	1.704	1.787	2.366	2.561
E/kcal mol^{-1}	5.755	5.045	8.274	7.295
T_0/K	104.62	157.88	88.43	124.79
RMSR	0.009	0.012	0.009	0.007

 This journal is © the Owner Societies 2012

Published on 16 January 2012 on http://pubs.rsc.org | doi:10.1039/C2CP23692C
Downloaded by University of Minnesota - Twin Cities on 04 March 2012

The MS-T conformational–rotational–vibrational partition functions have been used to obtain a multi-structural torsional factor $F^{\text{MS-T}}$ for the final rate constants calculations. The multidimensional zero-curvature tunneling (ZCT) and small-curvature tunneling (SCT) have been used for calculating transmission coefficients (κ). The single-structure harmonic (quasiharmonic) k^{CVT} rate constants were calculated on the potential energy surface obtained by the multi-configuration Shepard interpolation (MCSI) method using the lowest-energy structures of the reactant, product and transition state. Based on $F^{\text{SM-T}}$, κ^{MT}, and k^{CVT}, the final $k^{\text{MS-CVT/MT}}$ (MT can be ZCT or SCT) rate constants including both multi-structural torsional anharmonicity and multidimensional tunneling are obtained for both forward and reverse reactions. The present $k^{\text{MS-CVT/MT}}$ rate constants are the high-pressure limiting values. In the present investigations, we do not consider the pressure dependence of rate constants, but the reader is cautioned that pressure effects could be important because the barriers of the isomerization reactions involving all conformers are not high. However, our $k^{\text{MS-CVT/MT}}$ rate constants for the high-pressure limit provide modelers with an approximate upper limit of the rate constant at finite pressure.

The multi-structural torsional anharmonicity is found to be very important for the accurate rate constants calculations, especially for the reverse reaction because of the greater number of low-energy conformers located for the product. The reaction rate constants using the single-structural harmonic oscillator approximation are reduced by factors of 0.17 to 0.40 for the forward reaction and by factors of 0.017–0.066 for the reverse reaction. As a consequence there is also a very large effect on the equilibrium constant. A much larger effect is observed for multiple-structure anharmonicity than for torsional anharmonicity.

The tunneling effect and MS-T anharmonicity counteract each other at temperatures 385 K and 264 K for the forward and reverse reactions, respectively, and tunneling dominates at lower temperatures while MS-T anharmonicity dominates at higher temperatures.

The final $k^{\text{MS-CVT/SCT}}$ rate constants considering both small-curve tunneling and MS-T anharmonicity are believed to be more accurate rate constants than were previously available.

Acknowledgements

The authors are grateful to Tao Yu, Osanna Tishchenko, and John Alecu for help with the MCSI and MC-TINKERATE programs and for helpful discussions. This work was supported in part by the U. S. Department of Energy, Office of Science, Office of Basic Energy Sciences, under Grant No. DE-FG02-86ER13579 and as part of the Combustion Energy Frontier Research Center under Award Number DE-SC0001198.

References

1 (*a*) K. Y. Choo and S. W. Benson, *Int. J. Chem. Kinet.*, 1981, **13**, 833; (*b*) B. J. Finlayson-Pitts and J. N. Pitts Jr., *Chemistry of the Upper and Lower Atmosphere*, Academic Press, San Diego, 2000; (*c*) R. Atkinson and J. Arey, *Chem. Rev.*, 2003, **103**, 4605.
2 R. Atkinson, *Atmos. Environ.*, 2007, **41**, 8468.
3 (*a*) P. Morabito and J. Heicklen, *Bull. Chem. Soc. Jpn.*, 1987, **60**, 2641; (*b*) A. Heiss and K. Sahetchian, *Int. J. Chem. Kinet.*, 1996, **28**, 531; (*c*) H. Hein, A. Hoffmann and R. Zellner, *Phys. Chem. Chem. Phys.*, 1999, **1**, 3743; (*d*) P. Cassanelli, D. Johnson and R. A. Cox, *Phys. Chem. Chem. Phys.*, 2005, **7**, 3702.
4 (*a*) H. Somnitz and R. Zellner, *Phys. Chem. Chem. Phys.*, 2000, **2**, 1907; (*b*) R. Méreau, M. T. Rayez, F. Caralp and J. C. Rayez, *Phys. Chem. Chem. Phys.*, 2000, **2**, 1919; (*c*) L. Vereecken and J. Peeters, *J. Chem. Phys.*, 2003, **119**, 5159; (*d*) R. Méreau, M.-T. Rayez, F. Caralp and J.-C. Rayez, *Phys. Chem. Chem. Phys.*, 2003, **5**, 4828; (*e*) H. Somnitz, *Phys. Chem. Chem. Phys.*, 2008, **10**, 965; (*f*) J. Zheng and D. G. Truhlar, *Phys. Chem. Chem. Phys.*, 2010, **12**, 7782; (*g*) A. C. Davis and J. S. Francisco, *J. Am. Chem. Soc.*, 2011, **133**, 18208.
5 (*a*) B. C. Garrett and D. G. Truhlar, *J. Chem. Phys.*, 1979, **70**, 1593; (*b*) D. G. Truhlar and B. C. Garrett, *Acc. Chem. Res.*, 1980, **13**, 440; (*c*) D. G. Truhlar, A. D. Isaacson, R. T. Skodje and B. C. Garrett, *J. Phys. Chem.*, 1982, **86**, 2252; (*d*) D. G. Truhlar and B. C. Garrett, *Annu. Rev. Phys. Chem.*, 1984, **35**, 159; (*e*) A. Fernandez-Ramos, B. A. Ellingson, B. C. Garrett and D. G. Truhlar, in *Reviews in Computational Chemistry*, ed. T. R. Cundari and K. B. Lipkowitz, Wiley-VCH, Hoboken, NJ, 2007, vol. 23, p. 125.
6 (*a*) D.-h. Lu, T. N. Truong, V. S. Melissas, G. C. Lynch, Y.-P. Liu, B. C. Garrett, R. Steckler, A. D. Isaacson, S. N. Rai, G. C. Hancock, J. G. Lauderdale, T. Joseph and D. G. Truhlar, *Comput. Phys. Commun.*, 1992, **71**, 235; (*b*) Y.-P. Liu, G. C. Lynch, T. N. Truong, D.-h. Lu, D. G. Truhlar and B. C. Garrett, *J. Am. Chem. Soc.*, 1993, **115**, 2408.
7 (*a*) R. T. Skodje, D. G. Truhlar and B. C. Garrett, *J. Phys. Chem.*, 1981, **85**, 624; (*b*) R. T. Skodje and D. G. Truhlar, *J. Phys. Chem.*, 1981, **85**, 3019.
8 L. A. Curtiss, P. C. Redfern and K. Raghavachari, *J. Chem. Phys.*, 2007, **126**, 084108.
9 Z. Wigner, *Z. Phys. Chem., Abt. B*, 1932, **19**, 203.
10 (*a*) J. Zheng, T. Yu, E. Papajak, I. M. Alecu, S. L. Mielke and D. G. Truhlar, *Phys. Chem. Chem. Phys.*, 2011, **13**, 10885; (*b*) J. Zheng, T. Yu and D. G. Truhlar, *Phys. Chem. Chem. Phys.*, 2011, **13**, 19318; (*c*) T. Yu, J. Zheng and D. G. Truhlar, *Phys. Chem. Chem. Phys.*, 2012, **14**, 482.
11 (*a*) S. W. Benson, *Thermochemical Kinetics*, Wiley-Interscience, New York, 2nd edn, 1976; (*b*) T. Ni, R. A. Caldwell and L. A. Melton, *J. Am. Chem. Soc.*, 1989, **111**, 457; (*c*) N. Cohen, *J. Phys. Chem.*, 1992, **96**, 9052.
12 (*a*) T. Yu, J. Zheng and D. G. Truhlar, *Chem. Sci.*, 2011, **2**, 2199; (*b*) I. M. Alecu and D. G. Truhlar, *J. Phys. Chem. A*, 2011, **115**, 14599.
13 Y. Zhao and D. G. Truhlar, *J. Chem. Theory Comput.*, 2008, **4**, 1849.
14 (*a*) R. Krishnan, J. S. Binkley, R. Seeger and J. A. Pople, *J. Chem. Phys.*, 1980, **72**, 650; (*b*) T. Clark, J. Chandrasekhar, G. W. Spitznagel and P. v. R. Schleyer, *J. Comput. Chem.*, 1983, **4**, 294; (*c*) M. J. Frisch, J. A. Pople and J. S. Binkley, *J. Chem. Phys.*, 1984, **80**, 3265; (*d*) L. A. Curtiss, K. Raghavachari, C. Redfern, V. Rassolov and J. A. Pople, *J. Chem. Phys.*, 1998, **109**, 7764; (*e*) P. L. Fast, M. L. Sanchez and D. G. Truhlar, *Chem. Phys. Lett.*, 1999, **306**, 407; (*f*) B. J. Lynch, Y. Zhao and D. G. Truhlar, *J. Phys. Chem. A*, 2003, **107**, 1384.
15 J. Zheng, Y. Zhao and D. G. Truhlar, *J. Chem. Theory Comput.*, 2009, **5**, 808.
16 X. Xu, I. M. Alecu and D. G. Truhlar, *J. Chem. Theory Comput.*, 2011, **7**, 1667.
17 (*a*) K. Yang, Y. Zhao and D. G. Truhlar, *MN-GFM: Minnesota Gaussian Functional Module, version 5.0*, University of Minnesota, Minneapolis, MN, 2011; (*b*) M. J. Frisch, G. W. Trucks, H. B. Schlegel, G. E. Scuseria, M. A. Robb, J. R. Cheeseman, G. Scalmani, V. Barone, B. Mennucci, G. A. Petersson, H. Nakatsuji, M. Caricato, X. Li, H. P. Hratchian, A. F. Izmaylov, J. Bloino, G. Zheng, J. L. Sonnenberg, M. Hada, M. Ehara, K. Toyota, R. Fukuda, J. Hasegawa, M. Ishida, T. Nakajima, Y. Honda, O. Kitao, H. Nakai, T. Vreven, J. A. Montgomery, Jr., J. E. Peralta, F. Ogliaro, M. Bearpark, J. J. Heyd, E. Brothers, K. N. Kudin, V. N. Staroverov, R. Kobayashi, J. Normand, K. Raghavachari, A. Rendell, J. C. Burant, S. S. Iyengar, J. Tomasi, M. Cossi, N. Rega, J. M. Millam, M. Klene,

View Online

J. E. Knox, J. B. Cross, V. Bakken, C. Adamo, J. Jaramillo, R. Gomperts, R. E. Stratmann, O. Yazyev, A. J. Austin, R. Cammi, C. Pomelli, J. W. Ochterski, R. L. Martin, K. Morokuma, V. G. Zakrzewski, G. A. Voth, P. Salvador, J. J. Dannenberg, S. Dapprich, A. D. Daniels, Ö. Farkas, J. B. Foresman, J. V. Ortiz, J. Cioslowski and D. J. Fox, *GAUSSIAN 09 (Revision A.02)*, Gaussian, Inc., Wallingford, CT, 2009.

18 I. M. Alecu, J. Zheng, Y. Zhao and D. G. Truhlar, *J. Chem. Theory Comput.*, 2010, **6**, 2872.

19 (*a*) B. C. Garrett and D. G. Truhlar, *J. Phys. Chem.*, 1979, **83**, 1052; B. C. Garrett and D. G. Truhlar, *J. Phys. Chem.*, 1983, **87**, 4553(E); (*b*) B. C. Garrett and D. G. Truhlar, *J. Phys. Chem.*, 1979, **83**, 3058.

20 (*a*) D. C. Chatfield, R. S. Friedman, D. G. Truhlar, B. C. Garrett and D. W. Schwenke, *Faraday. Discuss. Chem. Soc.*, 1991, **91**, 289; (*b*) D. C. Chatfield, R. S. Friedman, D. G. Truhlar, B. C. Garrett and D. W. Schwenke, *J. Am. Chem. Soc.*, 1991, **113**, 486.

21 (*a*) D. G. Truhlar and A. Kuppermann, *J. Chem. Phys.*, 1970, **52**, 3842; D. G. Truhlar and A. Kuppermann, *J. Am. Chem. Soc.*, 1971, **93**, 1840; (*b*) B. C. Garrett, D. G. Truhlar, R. S. Grev and A. W. Magnuson, *J. Phys. Chem.*, 1980, **84**, 1730; B. C. Garrett, D. G. Truhlar, R. S. Grev and A. W. Magnuson, *J. Phys. Chem.*, 1983, **87**, 4554(E); (*c*) D. G. Truhlar, A. D. Isaacson and B. C. Garrett, in *The Theory of Chemical Reaction Dynamics*, ed. M. Baer, CRC Press, Boca Raton, FL, 1985, vol. 4, p. 65.

22 (*a*) K. S. Pitzer and W. D. Gwinn, *J. Chem. Phys.*, 1942, **10**, 428; (*b*) K. S. Pitzer, *J. Chem. Phys.*, 1946, **14**, 239; (*c*) D. G. Truhlar, *J. Comput. Chem.*, 1991, **12**, 266.

23 (*a*) R. P. Feynman and A. R. Hibbs, *Quantum Mechanics and Path Integrals*, McGraw-Hill, New York, 1965; (*b*) R. Q. Topper, *Adv. Chem. Phys.*, 1999, **105**, 117; (*c*) S. L. Mielke, J. Srinivasan and D. G. Truhlar, *J. Chem. Phys.*, 2000, **112**, 8768; (*d*) S. L. Mielke and D. G. Truhlar, *J. Chem. Phys.*, 2001, **114**, 621; (*e*) J. A. Miller, *Faraday Discuss.*, 2001, **119**, 461; (*f*) S. L. Mielke and D. G. Truhlar, *Chem. Phys. Lett.*, 2003, **378**, 317; (*g*) V. A. Lynch, S. L. Mielke and D. G. Truhlar, *J. Chem. Phys.*, 2004, **121**, 5148; (*h*) V. A. Lynch, S. L. Mielke and D. G. Truhlar, *J. Phys. Chem. A*, 2005, **109**, 10092.

24 A. D. Isaacson and D. G. Truhlar, *J. Chem. Phys.*, 1981, **75**, 4090.

25 J. Zheng, S. L. Mielke, K. L. Clarkson and D. G. Truhlar, *Comput. Phys. Commun.*, submitted.

26 (*a*) Y. Kim, J. C. Corchado, J. Villa, J. Xing and D. G. Truhlar, *J. Chem. Phys.*, 2000, **112**, 2718; (*b*) T. V. Albu, J. C. Corchado and D. G. Truhlar, *J. Phys. Chem. A*, 2001, **105**, 8465; (*c*) O. Tishchenko and D. G. Truhlar, *J. Chem. Theory Comput.*, 2007, **3**, 938; (*d*) M. Higashi and D. G. Truhlar, *J. Chem. Theory Comput.*, 2008, **4**, 790; (*e*) O. Tishchenko and D. G. Truhlar, *J. Chem. Theory Comput.*, 2009, **5**, 1454; (*f*) O. Tishchenko and D. G. Truhlar, *J. Chem. Phys.*, 2009, **130**, 024105.

27 (*a*) O. Tishchenko, M. Higashi, T. V. Albu, J. C. Corchado, Y. Kim, J. Vill, J. Xing, H. Lin and D. G. Truhlar, *MCSI-version 2010-1*, University of Minnesota, Minneapolis, MN, 2010; (*b*) J. W. Ponder, *TINKER-version 3.5*, Washington University, St. Louis, MO, 1997.

28 (*a*) T. V. Albu, O. Tishchenko, J. C. Corchado, Y. Kim, J. Villà, J. Xing, H. Lin, M. Higashi and D. G. Truhlar, *MC-TINKERATE-version 2008*, University of Minnesota, Minneapolis, MN, 2008; (*b*) J. C. Corchado, Y.-Y. Chuang, P. L. Fast, J. Villà, W.-P. Hu, Y.-P. Liu, G. C. Lynch, K. A. Nguyen, C. F. Jackels, V. S. Melissas, B. J. Lynch, I. Rossi, E. L. Coitiño, A. Fernandez-Ramos, J. Pu, T. V. Albu, R. Steckler, B. C. Garrett, A. D. Isaacson and D. G. Truhlar, *POLYRATE-version 9.1*, University of Minnesota, Minneapolis, MN, 2002.

29 J. Villà and D. G. Truhlar, *Theor. Chem. Acc.*, 1997, **97**, 317.

30 (*a*) N. L. Allinger, Y. H. Yuh and J. H. Lii, *J. Am. Chem. Soc.*, 1989, **111**, 8551; (*b*) J. H. Lii and N. L. Allinger, *J. Am. Chem. Soc.*, 1989, **111**, 8566; (*c*) J. H. Lii and N. L. Allinger, *J. Am. Chem. Soc.*, 1989, **111**, 8576; (*d*) N. L. Allinger, H. J. Geise, W. Pyckhout, L. A. Paquette and J. C. Gallucci, *J. Am. Chem. Soc.*, 1989, **111**, 1106; (*e*) N. L. Allinger, F. Li and L. Yan, *J. Comput. Chem.*, 1990, **11**, 848; (*f*) N. L. Allinger, F. Li, L. Yan and J. C. Tai, *J. Comput. Chem.*, 1990, **11**, 868.

31 (*a*) Y.-P. Liu, D.-h. Lu, A. Gonzalez-Lafont, D. G. Truhlar and B. C. Garrett, *J. Am. Chem. Soc.*, 1993, **115**, 7806; (*b*) A. Fernandez-Ramos and D. G. Truhlar, *J. Chem. Phys.*, 2001, **114**, 1491; (*c*) A. Fernandez-Ramos, J. A. Miller, S. J. Klippenstein and D. G. Truhlar, *Chem. Rev.*, 2006, **106**, 4518.

Downloaded by University of Minnesota - Twin Cities on 04 March 2012
Published on 16 January 2012 on http://pubs.rsc.org | doi:10.1039/C2CP23692C

 This journal is © the Owner Societies 2012